Sensors and Actuators B 193 (2014) 687–691

Contents lists available at ScienceDirect

Sensors and Actuators B: Chemical

journal homepage: www.elsevier.com/locate/snb

A precise pH microsensor using RF-sputtering IrO_2 and Ta_2O_5 films on Pt-electrode

Li-Min Kuo[a,c,*], Yi-Chia Chou[a], Kuan-Neng Chen[b], Chien-Chia Lu[a], Shuchi Chao[a]

[a] Department of Electrophysics, National Chiao Tung University, Hsinchu 300, Taiwan
[b] Department of Electronics Engineering, National Chiao Tung University, Hsinchu 300, Taiwan
[c] Department of Surgery, Medicine School, Stanford University, CA 95305, USA

ARTICLE INFO

Article history:
Received 18 May 2013
Received in revised form
11 November 2013
Accepted 26 November 2013
Available online 16 December 2013

Keywords:
IrO_2
Ta_2O_5
pH sensor
Proton–electron double injection
Solid-state sensor

ABSTRACT

In this study, an easily implemented surface modification scheme is reported employing Ta_2O_5 membrane which covers IrO_2 electrode in response to H^+ and eliminating redox species interference. Evidence shows that H^+ can pass through Ta_2O_5 films and react with IrO_2/Pt electrodes due to proton–electron double injection. A Ta_2O_5 membrane, an ionic conductor with an insulating property, blocks the transport of electrons generated from oxygen perturbation in the solution. The conduction of both electrons and protons preserve the current continuity across the interface. Owing to proton–electron double injection, IrO_2 will be reduced to $Ir(OH)_3$ during pH detection. The $[IrO_2]/[Ir(OH)_3]$ will remain constant and therefore the Nernstian electrode potential performs stably as a function of pH (−59.447 to −59.504 mV/pH, 2 < pH < 13). In addition, the proposed pH microsensor displayed high ion selectivity with respect to K^+, Na^+, and Li^+, with log $K_{H,M}$ values (∼−12.4) and has a working lifetime over one week.

1. Introduction

Unlike bulky pieces of laboratory equipment used previously, miniature microchips for pH detection offer a number of merits such as compact chip size, rapid response time, and excellent compatibility in a microsystem [1,2]. To provide an H^+-sensitive microsensor that can perform precisely with reactants for chemical and biological applications is critical, as we have to incubate cells with ultra-small volumes in an isolated and sterilized environment [2]. The solid ion-to-electron transducers have been utilized in the conventional configuration by immobilizing conductive copolyaniline nanoparticles in a vinyl resin matrix, improving upon disadvantages of conventional PVC (poly(vinyl chloride)) membranes [3–6]. Metal-oxides (MO_x) behave as mixed electronic and ionic conductors due to their oxygen defect stoichiometry and have been considered as pH-sensor materials over past decades [7–9]. RuO_2, SnO_2 and IrO_2 are the most promising materials due to their chemical stability and high conductivity [10–14]. Because of the instability and relative freedom from interference, iridium oxides (IrO_x) have been employed in many researches [12–16]. However, the inherent drawbacks still exist in conventional IrO_2-coated electrodes such as the incomplete oxidation film (IrO_{2-x}), which will easily react to oxygen, thereby degrading the long-term stability of the interface potential.

In this study, a stacked structure, different from conventional structures of metal oxides, was used to detect the interfacial pH levels of medium acidity. A sputtering IrO_2 film was used in conjunction with patterned electrodes to produce a conductive pH sensor. With inherent immunity to O_2 perturbation, an encapsulation layer of Ta_2O_5 film was used to cover the IrO_2/Pt microsensor [17]. Ta_2O_5 film using an RF-sputtering method was stacked on IrO_2 film to alleviate perturbations from experimental fluctuations [18–20] and improved the microsensor performance significantly. The proposed solid-state microsensor exhibited good stability and repeatability in various pH environments ranging from pH = 2.01 to 13.01.

2. Experimental

The microsensor, schematically described in Fig. 1(a), was fabricated by sputtering of IrO_2 and Ta_2O_5 films on Pt electrodes. An *n*-type wafer (4-in. and 10–20 Ω-cm) was cleaned in piranha solution (H_2SO_4:H_2O_2 = 3:1) at 80 °C for 20 min, and followed by a deionized water rinse for 5 min. A 5000 Å SiO_2 was deposited by a wet-oxidation process on the Si substrate, followed by a LPCVD-grown Si_3N_4 (6000 Å). Next, 50 Å of chromium followed by Pt (1200 Å) layer was deposited on the Si_3N_4 film by a dual

* Corresponding author at: Department of Electrophysics, National Chiao Tung University, Hsinchu 300, Taiwan. Tel.: +886 3571212156144; fax: +886 35725230.
E-mail addresses: lmkuo.ep97g@nctu.edu.tw, lmkuo@ieee.org (L.-M. Kuo).

0925-4005/$ – see front matter © 2013 Elsevier B.V. All rights reserved.
http://dx.doi.org/10.1016/j.snb.2013.11.109

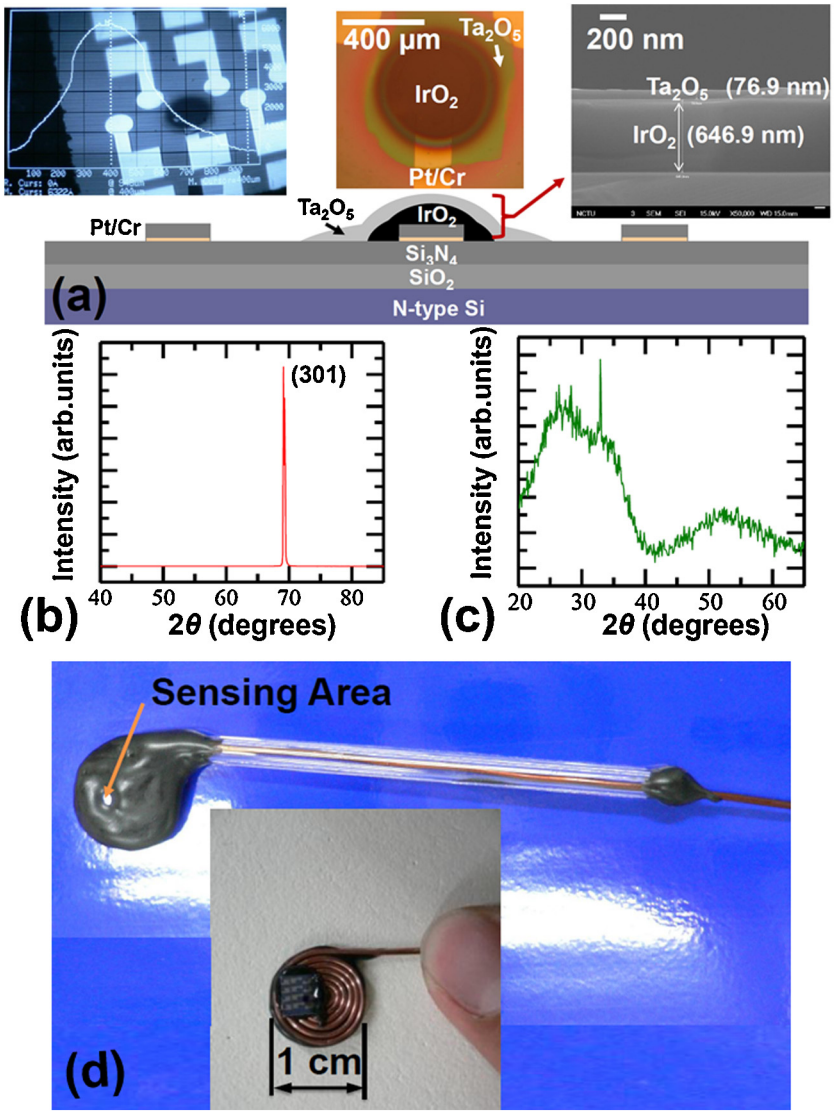

Fig. 1. (a) Schematic shows the cross-sectional structure of our pH sensor. Left-top inset is the profile of the stacked structure scanned by a surface profilometer (Dektak 3030); Middle-top inset displays top view of the pH-sensor captured by a microscopic micrograph; Right-top inset shows cross-sectional view of SEM (scan electron microscope) image toward the stacked structure of our pH-sensor; The IrO_2 and Ta_2O_5 thickness are 646.9 nm and 76.9 nm, respectively. (b) The X-ray diffraction (XRD) pattern of polycrystalline IrO_2 film. (c) The X-ray diffraction (XRD) pattern of amorphous Ta_2O_5 film. (d) Sensor with the holder loaded into a glass-tube and sealed on two terminals with the insulating epoxy (Inset: the holder made of Cu wire for the attachment of the pH-sensor and the electrical contact for individual Pt-electrode connected using Ag epoxy).

electron-beam evaporator and then patterned using a lift-off technique. The Pt-electrodes, separated by a distance of 400 μm, were typically 600 μm wide and 1400 μm long (excluding the lead portion with a diameter of 400 μm) as utilized as before [21,22]. The chip surface was cleaned in sequence with deionized water, trichloroethane, acetone, and deionized water in an ultrasonic cleaner. Then, the chip was purged with a dry N_2 jet, followed by a dehydration bake at 120 °C for 30 min. The IrO_2 film (6500 Å) was fabricated using sputtering of an iridium target (99.95% and 21.8 g/cm^3) at a total pressure of 90 mTorr (50% O_2 in Ar) as similar as described earlier [22]. Sputtering of the Ta_2O_5 target (99.95% and 4.77 g/cm^3) was carried out (50% O_2 in Ar) at a total pressure of 60 mTorr. The X-ray diffraction (XRD) patterns of the sputtered IrO_2 and Ta_2O_5 films are shown in Fig. 1(b) and (c), respectively (Fig. S1 in Supporting Information). The electrical contacts for individual Pt-electrodes were made using Ag epoxy (FA-705, Fujikura Kasei), which were later encapsulated using an insulating epoxy for preventing short circuits, as shown in Fig. 1(d).

The potential-difference characteristics of the microsensor were measured by a Keithley Programmable Electrometer (Model 617). All potentials of our pH-sensor were measured relative to SCE (Saturated Calomel Electrode, Z11311-5, Aldrich) and the commercial pH-meter (Mettler-Delta 350) was used as a benchmark in the experiments (Fig. S2 in Supporting Information). A GPIB (General Purpose Interface Bus) interface and a LabView-based program were employed for recording all of the experimental results. To maintain the constant temperature in the experiment, a water-circulating system was connected to the inlet and outlet of the beer-cooler container. A thermal-couple meter (Fluke-714) was used for monitoring the operation temperature. Before measurements were commenced, a two-point calibration using pH-calibration buffers (pH = 4, 7, and 10) was required. The pH-levels of sample solutions were prepared using different concentrations of Britton–Robinson buffer solution consisted of 0.04 M H_3BO_3, 0.04 M H_3PO_4 and 0.04 M CH_3COOH mixture; twelve samples were titrated to the desired pH-value (from pH = 2 to 13) with 0.2 M KOH pseudo-randomly dropping.

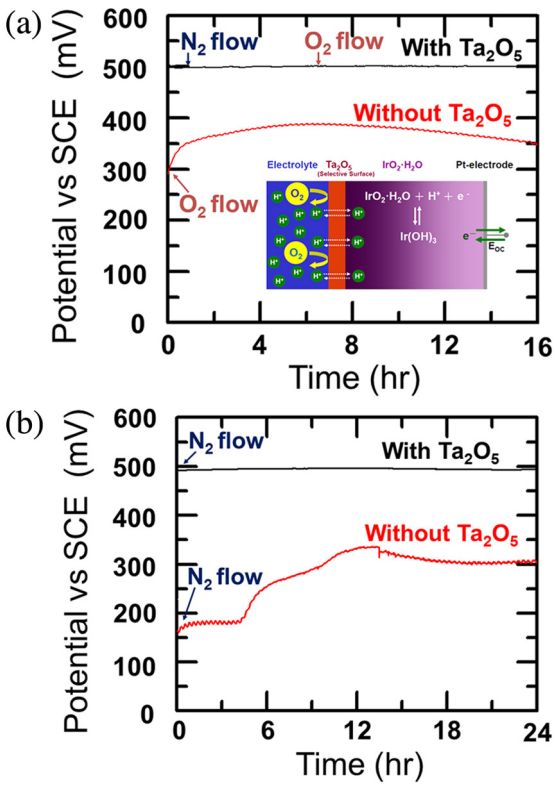

Fig. 2. (a) The IrO_2/Pt-electrode sensor with/without Ta_2O_5 film and measured at pH = 4.01 and 19 °C: plot of potential difference versus time under the abundant O_2 situation. (Inset illustrates schematically the pH-response mechanism for the transport of carriers across the encapsulation interface.) (b) The IrO_2/Pt-electrode sensor with/without Ta_2O_5 film and measured at pH = 4.01 and 19 °C. Plot of potential difference versus time under supplying abundant N_2 gas continuously at the beginning of the experiment.

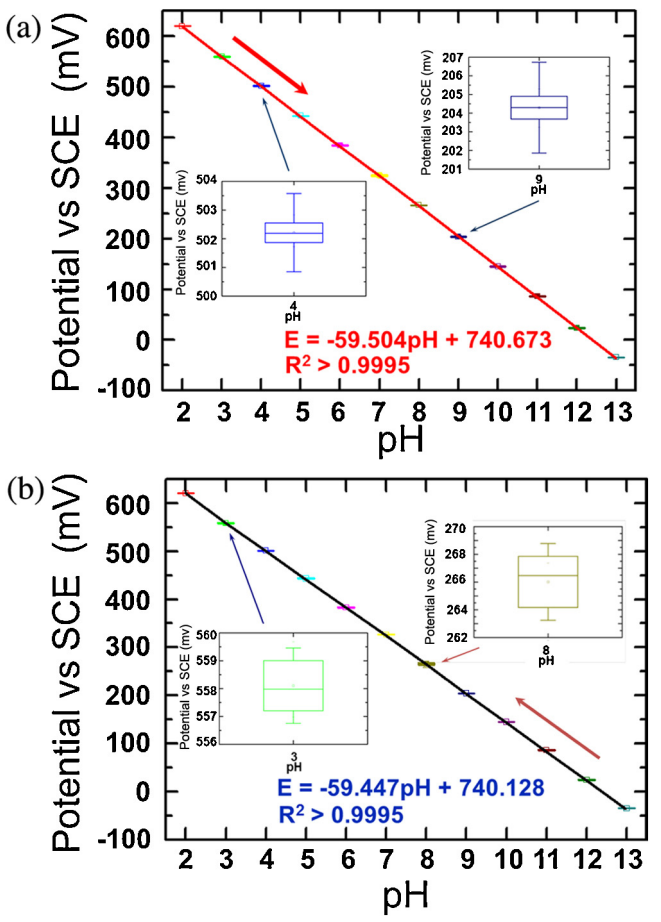

Fig. 3. Reversibility characteristic according to the fitting-slope plots with error bars at room temperature (a) pH = 2.01–13.01; 10 points from the 10 forward measurements; the fitting slope of the forward measurement is −59.504 mV/pH and the intercept value at pH = 0 indicates E^O is 740.673 mV. (b) pH = 13.01 to 2.01; 10 points from 10 backward measurements. The fitting slope of the backward measurement is −59.447 mV/pH and the intercept value is 740.128 mV.

3. Results and discussion

In Fig. 1(b), the XRD pattern indicates that the IrO_2 grains are made of well-developed crystals and the grains are more oriented in the (3 0 1) direction. The diffraction angle of the XRD is 69.1° and the grain size of IrO_2 film is 107.16 nm, which is derived using Scherrer's equation [23]. The XRD analysis of Fig. 1(c) shows that the amorphous film of Ta_2O_5 encapsulation layer providing larger reaction surface area of the microsensor was covered on the IrO_2 sensor and offers the selective membrane function of H^+ ions during the measurement.

IrO_2-reductions to insulating $Ir(OH)_3$ occurred at more positive electrochemical potentials in acidic media between pH = 2 and 13. (Reaction (1))

$$IrO_2 \cdot \chi H_2O \ \ (\text{conductor}) + H^+ + e^- \leftrightarrow Ir(OH)_3 \ \ (\text{insulator}) \qquad (1)$$

The concentration ratio of $IrO_2{\cdot}H_2O$ (oxidized form) versus $Ir(OH)_3$ (reduced form) will be affected as they are redox by other materials. The redox transformations arise due to the insertion of ionic species migrating from the surface into the interior of IrO_2 and can produce large conductance changes. According to Nernstian response, the pH-potential sensitivity will be −59.05 mV/pH and the redox potential is determined by Eq. (2).

$$E = E^O - \frac{RT}{F} \ln \frac{[IrO_2][H^+]}{[Ir(OH)_3]} = E^O - 2.303\frac{RT}{F}\text{pH}$$

$$= E^O - 0.05905\text{pH} \qquad (2)$$

where R = 8.3147 J/K-mol; T = 298 K; F = Faraday constant; E^O represents the standard potential of IrO_2.

N_2 gas was supplied into the solution buffer to replace O_2, which may contribute voltage fluctuations on the sensor surface [17]. The comparison plots of potential difference versus time are shown in Fig. 2(a) and (b). Significant improvements, a stable potential-difference versus SCE of 496 mV in an acid solution (pH = 4.01) over 16 h, were produced by the microsensor with the additional Ta_2O_5 film, as shown in Fig. 2(a). In Fig. 2(b), under supplying abundant nitrogen gas in the solution, the potential difference of the microsensor without the Ta_2O_5 encapsulation layer shows stable potential difference after 24 h. The potential deviations may be caused by some factors such as the oxidation states from incomplete oxidation (IrO_{2-x}) and the surface ion-exchanges in iridium oxides [9]. These non-ideal effects will produce surface charge variations with time and generate a new equilibrium after each reaction [24]. The time (t_0) for the transport of H^+ passing through Ta_2O_5 film will be longer according to $t_0 = L^2/6D$ [25] when the thicker Ta_2O_5 film is deposited. (D is diffusivity and L is the membrane thickness) Additionally, a thicker Helmholtz layer generated at the interface of the encapsulation layer will cause longer transient-response time [26]. In our experiments, the potential difference versus SCE is kept at zero for over 6 h with the deposited Ta_2O_5 film of 600 nm. The response and recovery time are defined as 10–90% of the rising and falling edge in the transient response. The maximum ramp-up and recovery time are within 15 s as we change the sample solutions (from pH = 2 to 13 and from pH = 13 to 2).

Table 1
The performance comparison of our microsensor and other pH sensors.

	Sensitivity (mV/pH)	Operation range (pH)	Calibration needed	Sensor size (mm^2)	Long-term stability (mV/h)	Ref
ISFET-based sensor	55–58	2–12	No	<1	<15	[29,30]
Thick-film sensor	~47	4–10	Yes	<2.5	<0.5	[31]
Conventional glass electrode	~59	0–14	Yes	>100	<0.1	[32]
IrO2-based electrode	72.5–75	2–11	No	<32	<0.5	[7]
This work	~59.5	2–13	No	<0.8	<0.1	N/A

The reversibility and reproducibility measurements were carried out by placing our pH microsensor in the sample solutions (twelve pH-levels). The microsensor was first immersed into the pH = 2 solution and then successively processed in the solution from pH = 3.01 to 13.01 and reversed back from pH = 13.01 to 2.01. A magnetic stir bar on the bottom of the beaker was used to minimize the effect from surface-junction potentials [27]. The experiments of the forward and backward pH measurements were processed repeatedly for 10 loops at room temperature. From the forward (pH = 2.01 → 13.01) and backward (pH = 13.01 → 2.01) measurements, the RMS (root mean square) value of each pH level was calculated using the obtained 10 points from 10 loop-cycle scans. The measurement results with error bars are illustrated statistically in Fig. 3(a) and (b). The slope discrepancy (~57 μV/pH) between the forward and backward measurements may be due to manual-operation errors and dynamic processes of ion neutralization called the effect of liquid junction potential [22,26]. The long-term performance during the five days of experiments were processed (pH = 4.01 for 12 h and then followed by pH = 7.01 for 12 h). In Fig. 4, the experiment was processed in sequence from pH = 2.10 to 13.01 and each duration of one pH-level measurement was lasted for 30 s. Similarly, the results of pH = 13.01 to 2.01 were also captured accordingly. Potential differences (RMS) versus SCE are 494.6–498.1 mV at pH = 4.01 and 314.3–320.6 mV at pH = 7.01 (Table S1 in Supporting Information). At pH = 4.01, the fitting slopes of potential difference versus temperature from 20 to 17 °C and 17 to 50 °C are −2.48 mV/°C and 2.18 mV/°C, respectively. The theoretical value is −0.796 mV/°C (pH = 4.01) derived from Eq. (2).

The cation interferences of the microsensor selectivity were conducted with the fixed interference method (FIM) in pH measurements. According to the Nikolsky–Eisenman equation [28], the interference effects from different ions (Na^+, K^+, and Li^+) were calculated with the potentiometric selective coefficients by Eq. (3).

$$E = C + \left(\frac{RT}{z_A F}\right) \times \ln(a_A + K^{pot}_{A,B}(a_B)^{z_A/z_B} + K^{pot}_{A,C}(a_C)^{z_A/z_C} + \cdots) \quad (3)$$

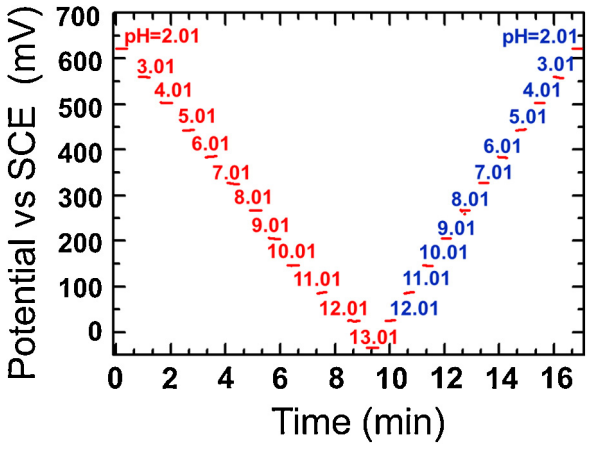

Fig. 4. Plot of time-dependent pH response steps for the pH detection from pH = 2 to 13 and from pH = 13 to 2.

where E denotes the measured electromotive force; C is a constant; a_A, a_B and a_C are the concentrations of the primary ion A, interfering ion B and C, respectively; z_A, z_B and z_C are the charge numbers of the principal ion A, interfering ion B and C; R = 8.3147 J/K-mol; T = 298 K; F = Faraday constant.

The cations were used to compare the interference effects in potentiometric measurements of the selectivity coefficient. The interference cation agents (0.1 M of NaCl, 0.1 M of KCl, and 0.1 M of LiCl) were added separately into sample solutions at different pH levels of a test buffer solution. The sensitivity was measured before and after the interference agent was added at room temperature. The presence of the cations (Li^+, Na^+, and K^+) changed slightly the sensitivity slopes from −59.5 mV/pH to −59.23, −59.02, and −59.62 mV/pH, respectively. The selectivity coefficients for lithium, sodium, and potassium cations were 2.63×10^{-13}, 4.67×10^{-13} and 3.47×10^{-13} (Table S2 in Supporting Information).

Table 1 tabulates a comparison of this work with respect to other conventional pH sensors. The points of merit for the proposed microsensor performance are characterized in terms of sensitivity, operation range, sensor size, and long-term stability. The microsensor exhibits compatible long-term stability compared with the performance of the conventional glass electrode. Additionally, the microsensor offers a number of merits such as compact chip size, rapid response time, and ease of fabrication.

4. Conclusions

In this study, a new solid-state pH sensor made of sputtering IrO_2 and Ta_2O_5 films in response to the presence of H^+ has been reported. With inherently robust immunity to O_2 perturbation, the encapsulation layer of Ta_2O_5 film fully covered the IrO_2/Pt electrodes and prevented $[IrO_2]/[Ir(OH)_3]$ from being increased in Nernstian response. Mimicking a bipolar ion-exchange membrane, the IrO_2 film covering a Pt-electrode acted as a mixed electronic and ionic conductor. By reacting with H^+ passing through Ta_2O_5 film, the bending of the Fermi-level of the IrO_2 film will produce a space charge layer. The conductivity will be controlled according to proton–electron double injection. Apart from its linear temperature-dependent characteristic and good reliability, its sensitivity shows only slight and negligible discrepancy compared with theoretical Nernstian response. This solid-state microsensor exhibits the good stability and repeatability in various pH environments (from 2.01 to 13.01) at room and higher temperature. This pH-sensitive microsensor will be useful as a basis for the construction of durable microsensors for tracing the acidity in environmental and biological applications.

Acknowledgement

The corresponding author appreciates for supporting the scholarship from Chung-Shan Institute of Science and Technology (CSIST), Taoyuan, Taiwan and National Defense Industrial Development Foundation (NDIDF), Taipei, Taiwan. The authors express special thanks to the writing support from Ms. Holli Kinstle at Language Teaching and Research Center of National Chiao Tung University, Hsinchu, Taiwan.

Appendix A. Supplementary data

Supplementary material related to this article can be found, in the online version, at http://dx.doi.org/10.1016/j.snb.2013.11.109.

References

[1] S.M. Sze, Semiconductor Sensors, John Wiley & Sons, New York, 1994.
[2] M.L. Schuler, F. Kargi, Bioprocess Engineering-Basic Concepts, Prentice Hall, Englewood Cliffs, NJ, 1992.
[3] A.J. Michalska, C. Appaih-Kusi, L.Y. Heng, S. Walkiewicz, E.A.H. Hall, An experimental study of membrane materials and inner contacting layers for ion-selective K^+ electrodes with a stable response and good dynamic range, Analytical Chemistry 76 (2004) 2031–2039.
[4] L.Y. Heng, E.A.H. Hall, Taking the plasticizer out of methacrylic-acrylic membranes for K^+-selective electrodes, Electroanalysis 12 (2000) 187–193.
[5] X.G. Li, H. Feng, M.R. Huang, G.L. Gu, M.G. Moloney, Ultrasensitive Pb(II) potentiometric sensor based on copolyaniline nanoparticles in a plasticizer-free membrane with a long lifetime, Analytical Chemistry 84 (2012) 134–140.
[6] M.R. Huang, X.W. Rao, X.G. Li, Y.B. Ding, Lead ion-selective electrodes based on polyphenylenediamine as unique solid ionophores, Talanta 85 (2011) 1575–1584.
[7] S.A.M. Marzouk, Improved electrodeposited iridium oxide pH sensor fabricated on etched titanium substrates, Analytical Chemistry 75 (2003) 1258–1266.
[8] P. Kurzweil, Metal oxides and ion-exchanging surfaces as pH sensors in liquids: state-of-the-art and outlook, Sensors 9 (2009) 4955–4985.
[9] A. Fog, R.P. Buck, Electronic semiconducting oxides as pH sensors, Sensors and Actuators 5 (1984) 137–146.
[10] Y.H. Liao, J.C. Chou, Preparation and characteristics of ruthenium dioxide for pH array sensors with real-time measurement system, Sensors and Actuators B 128 (2007) 603–612.
[11] C.N. Tsai, J.C. Chou, T.P. Sun, S.K. Hsiung, Study on the sensing characteristics and hysteresis effect of the tin oxide pH electrode, Sensors and Actuators B 108 (2005) 877–882.
[12] G.M. da Silva, S.G. Lemos, L.A. Pocrifka, P.D. Marreto, A.V. Rosario, E.C. Pereira, Development of low-cost metal oxide pH electrodes based on the polymeric precursor method, Analytical Chimica Acta 616 (2008) 36–41.
[13] J. Hendrikese, W. Olthuis, P. Bergveld, A method of reducing oxygen induced drift in iridium oxide pH sensor, Sensors and Actuators B 53 (1998) 97–103.
[14] P.J. Kinlen, J.E. Heider, D.E. Hubbard, Solid-state pH sensor-based on a Nafion-coated Iridium oxide indicator electrode and a polymer-based silver-chloride reference electrode, Sensors and Actuators B 22 (1994) 13–25.
[15] S. Marzouk, S. Ufer, R. Buck, T. Johnson, L. Dunalp, W. Cascio, Electrode-posited iridium oxide pH electrode for measurement of extracellular myocardial acidosis during acute ischemia, Analytical Chemistry 70 (1980) 5054–5061.
[16] I.A. Ges, K.P.M. Currie, F. Baudenbacher, Electrochemical detection of catecholamine release using planar iridium oxide electrodes in nanoliter microfluidic cell culture volumes, Biosensors and Bioelectronics 34 (2012) 30–36.
[17] L. Bousse, S. Mostarshed, B. Van Der Schoot, N.F. de Rooij, Comparison of the hysteresis of Ta_2O_5 and Si_3N_4 pH-sensing insulators, Sensors and Actuators B 17 (1994) 157–164.
[18] C. Bartic, A. Campitelli, S. Borghs, Field-effect detection of chemical species with hybrid organic/inorganic transistors, Applied Physics Letters 82 (2003) 475–477.
[19] Y. Abe, N. Itadani, M. Kawamura, K. Sasaki, H. Itoh, Ion conducting properties of hydrogen-containing Ta_2O_5 thin films prepared by reactive sputtering, Vacuum 83 (2009) 528–530.
[20] U. Teraninthom, Y. Miyahara, T. Moriizumi, The suitability of Ta_2O_5 as a solid state ion-sensitive membrane, Japanese Journal of Applied Physics 26 (1987) 2112–2120.
[21] L.M. Kuo, Y.T. Shih, C.S. Wu, Y.C. Lin, S.C. Chao, A new hybrid method for H_2S-sensitive devices using WO_3-based film and ACF interconnect, Measurement Science and Technology 24 (2013) 0751051–0751057.
[22] L.M. Kuo, K.N. Chen, Y.L. Chuang, S. Chao, A flexible pH-sensing structure using WO_3/IrO_2 junction with Al_2O_3 encapsulation layer, ECS Solid State Letters 2 (2013) 28–30.
[23] A.L. Patterson, The Scherrer formula for X-ray particle size determination, Physical Review 56 (1939) 978–982.
[24] W. Olthuis, M.A.M. Robben, P. Bergveld, M. Bos, W.E. Linden, pH sensor properties of electrochemically grown iridium oxide, Sensors and Actuators B 2 (1990) 247–256.
[25] J. Crank, G.S. Park, Diffusion in Polymers, Academic Press, London, 1968.
[26] A.J. Bard, Electrochemical Methods: Fundamentals and Application, John Wiley & Sons, New York, 2006.
[27] J. Lyklema, Fundamentals of Interface and Colloid Science 2 (1995) 3208.
[28] D.G. Hall, Ion-selective membrane electrodes: a general limiting treatment of interference effects, Journal of Physical Chemistry 100 (1996) 7230–7236.
[29] S.V. Dzyadevych, A.P. Soldatkin, A.V. El'skaya, C. Martelet, N. Jaffrezic-Renault, Enzyme biosensors based on ion-selective field-effect transistors, Analytica Chimica Acta 568 (2006) 248–258.
[30] J.L. Chiang, S.S. Jan, J.C. Chou, Y.C. Chen, Study on the temperature effect, hysteresis and drift of pH-ISFET devices based on amorphous tungsten oxide, Sensors and Actuators B 76 (2001) 624–628.
[31] A. Gac, J.K. Atkinson, Z. Zhang, R.P. Sion, A comparison of thick-film chemical sensor characteristics in laboratory and on-line industrial process applications, Measurement Science and Technology 13 (2002) 2062–2073.
[32] http://www.wtw.de/en/products/lab/ph.html

Biographies

Li-Min Kuo was born in Taiwan. Dr. Kuo recieved his Ph.D degree in science from National Chiao Tung University, Hsinchu, Taiwan. His current research interests include biosensor design and fabrication, tissue engineering, and microsystem fabrication in the biological applications.

Yi-Chia Chou is an assistant professor of Department of Electrophysics in National Chiao Tung University. Prof. Chou received her B.Sc. degree in Materials Science and Engineering from National Tsing Hua University, Hsinchu, Taiwan and Ph.D. degree from University of California at Los Angeles. Her current research interests include controlled growth of Si/Ge heterojunction nanowires using novel catalysts, and applications of one-dimensional periodic silicide/Si heterostructures.

Kuan-Neng Chen is currently a professor of Department of Electronics Engineering in National Chiao Tung University, Hsinchu, Taiwan. Dr. Chen received his Ph.D. degree in Electrical Engineering and Computer Science and his M.S. degree in Materials Science and Engineering from Massachusetts Institute of Technology (MIT), respectively. Prior to the faculty position, he was a Research Staff Member and Project Leader at the IBM Thomas J. Watson Research Center. Dr. Chen has received several IBM Awards, including five IBM Invention Plateau Invention Achievement Awards and two Awards from Exploratory Technology Group. He has authored and coauthored more than 140 publications in book chapters, journals and international conference proceeding, and holds more than 70 patents or patent applications. He is currently the committee member of IMAPS 3D Packaging. He is a member of Phi Tau Phi Scholastic Honor Society. His current interests are three-dimensional integrated circuits (3D IC), through-silicon via (TSV) technology, wafer bonding technology, phase-change material devices, nano devices.

Chien-Chia Lu obtained his B.Sc. degree in Physics and received his M.Sc. in Electrophysics from National Chiao Tung University.

Shuchi Chao is an associate professor of Department of Electrophysics in National Chiao Tung University. Prof. Chao received his Ph.D. degree from Massachusetts Institute of Technology (MIT). His current interests are microsensor fabrication, and electrochemical physics.